Smart Tone Reproduction of Digital Images

Dun-Yu Hsiao and Hong-Yuan Mark Liao

Smart Tone Reproduction of Digital Images

Dun-Yu Hsiao and Hong-Yuan Mark Liao

Institute of Information Science

Academia Sinica, Taipei, Taiwan 115

+886-2-27883799 Ext 1550

silverseraph@gmail.com, liao@iis.sinica.edu.tw

Abstract—In this paper, we propose an effective scheme for enhancing the visual details of digital images with the minimal amount of user adjustment. Digital archives are becoming increasingly popular due to the development of convenient and powerful digitizing techniques. However, a substantial number of digital images suffer from loss of detail because they were captured with old-fashioned equipment. Thus, an automatic tone reproduction technique is needed. We attempt to solve the above issues by combining a novel local normalization concept with an adaptive contrast assessment process. The proposed tone reproduction scheme effectively enhances poor quality regions, while simultaneously preserving good quality regions with default parameter settings. As the proposed scheme eliminates most of the manual effort required to adjust the parameters, it can be considered as nearly automatic. The results of experiments demonstrate that the scheme outperforms many existing algorithms when applied to restoring digital images for a national digital archive program.

Index Terms—Detail preserving, tone reproduction

1. INTRODUCTION

The lack of sufficient dynamic range and proper shading conditions remain challenging issues for modern sensor technology and photography. Under different lighting conditions, a digital sensor can only capture a limited dynamic range because it is not as sensitive as the human eye. Brightness that falls beyond the sensor's linear dynamic range will be compressed and become imperceptible to humans. In recent years, a number of tone reproduction algorithms have been developed to compensate for a digital sensor's inability to genuinely reproduce images that the human eye can see [1-7]. Depending on the strategies employed, existing techniques can be classified into two categories: global tone reproduction and regional tone reproduction methods. Several global tone reproduction approaches have been developed. For example, Fattal *et al.* [3] proposed a method that suppresses the magnitude of large luminance gradients and preserves fine details by identifying changes in intensity. Then, by solving a Poisson equation on the modified gradient field, the larger gradients are reduced and an image with low dynamic range is produced. In [2], Durand *et al.* proposed a bilateral filter that decomposes an image into two layers: a large-scale variation base layer and a visibility preserving detail layer. The two layers are produced by applying bilateral filtering, and the relative contrast is subsequently reduced in the large-scale variation layer. Pattanaik *et al.* [1] developed a computational model of human adaptation and spatial vision for realistic tone reproduction. In contrast, Drago *et al.* [4] proposed a method based on the logarithmic compression of luminance values that produces images with well-preserved details and satisfactory contrast levels. Unfortunately, the drawback of all existing global approaches is that they inevitably suppress high contrast regions.

For regional tone reproduction, Krawczyk *et al.* [6] proposed decomposing an image into areas of consistent luminance and calculating the local brightness values; while Chen *et al.* [7] developed another region-based method that applies bilateral techniques on different image regions to obtain better quality images. Since region contrast reproduction schemes process each image region differently, the main limitation of such approaches is that they tend to produce unnatural boundaries. Moreover, a common problem with global and regional tone reproduction approaches is that the quality of their results depends to a large extent on how the parameters are set.

To resolve the above-mentioned issues, we propose a method that uses two primary components—local normalization and adaptive contrast assessment. For local normalization, our approach starts by identifying an image's local maximum and minimum surfaces. By considering an image as a 3D surface, the local maxima and local minima surface patches can enclose the entire image's 3D surface from above and below. Then, by normalizing the image toward the local maxima and minima, we can expand the image signal to increase the utilization of its dynamic range. After local normalization, our scheme implements an adaptive contrast assessment process that adaptively blends each pixel of the locally normalized image into the original image. Combining local normalization and adaptive contrast assessment allows us to enhance poor quality regions directly, while simultaneously preserving good quality regions—just as photographers do in manual image enhancement. In addition, since the set of parameters in our scheme are pre-determined (discussed in Section 2.4), users do not need to adjust the parameter settings further. This feature is especially important when applying our algorithm to digital archiving tasks that deal with huge amounts of data.

The remainder of this paper is organized as follows. In the next section, we introduce the proposed method and elaborate on our scheme's design. Section 3 details our experiment results and evaluations, and Section 4 contains some concluding remarks.

2. THE PROPOSED METHOD

In this section, we introduce the primary concepts and the algorithm of the proposed method. We consider the characteristics and the goal of our general tone reproduction method in Section 2.1 and discuss the design of the algorithm in Section 2.2. The methods used to evaluate the effectiveness of our tone reproduction scheme are presented in Section 2.3. Then, in Section 2.4 we analyze our tone reproduction scheme.

2.1. The Design Concepts

We start by analyzing the effect and purpose of general image enhancement and tone reproduction in order to devise our novel tone reproduction algorithm. An image model $I(x, y)$ is commonly regarded as a product of the reflectance $R(x, y)$ and the luminance $L(x, y)$ of a pixel (x, y), i.e.,

$$I(x, y) = R(x, y) \times L(x, y).$$ (1)

Thus, the enhanced image $I'(x, y)$ can be represented as

$$I'(x, y) = R'(x, y) \times L'(x, y).$$ (2)

When enhancing an image, by using use homomorphic filtering for example, the filter suppresses the luminance part of the image such that the overall contrast is reduced and the corresponding histogram converges toward the center of a dynamic range. To verify this phenomenon, we also manually enhanced over 250 poorly captured images to determine whether such a characteristic meets human expectations. Through both the mathematical model and observations of manual enhancements, we found that, generally, the set of enhanced images exhibited low distributions at both extremes of a histogram. We express this characteristic as follows:

$$G_{\min} + \delta < L'(x, y) < G_{\max} - \phi,$$ (3)

where $G_{\min}$ and $G_{\max}$ are the respective minimum and maximum values of a dynamic range; and δ and ϕ are two positive constants that show $L'(x, y)$ will not become extreme luminance values of the dynamic range. On the other hand, using homomorphic filtering to enhance image details increases the ratio of reflectance $R(x, y)$ to luminance $L(x, y)$. Again, by examining the set of manually enhanced images, we found that the resultant contrasts were larger in the enhanced images than in the originals. Weber's Law and many other just noticeable difference (JND) profiles also allude to a similar phenomenon; i.e., a contrast is only perceivable when it is greater than a certain threshold. Therefore, it is reasonable to assume that an image's details are only visible when its local contrast is large enough. Formally, the above-mentioned characteristics can be expressed as follows:

$$\frac{R'(x, y)}{L'(x, y)} > \frac{R(x, y)}{L(x, y)},$$ (4)

$$Contrast\,(I(x, y)) > threshold,$$ (5)

-4-

where the contrast between details is larger than the threshold constrained by Weber's Law or JND profiles to ensure that it is perceivable by the human eye. Taken together, Equations (3), (4), and (5) can function as guidelines for designing image enhancement algorithms. To extend the range of reflectance $R(x, y)$, we utilize the dynamic range as much as possible to ensure simultaneous satisfaction of Equations (4), and (5). Based on this concept, we include a normalization algorithm in our scheme to increase the usage of the dynamic range. Furthermore, the constraint in Equation (3) can be satisfied by modifying the normalization stage into a local normalization stage. For example, a signal can be considered as having S piecewise densely connected line segments, which can be expressed as follows:

$$
\begin{aligned}
&I(x, y) = \{I_k(x, y), \ k = 1, 2, ..., S\}, \\
&I_k(x, y) = I_{\min,k} + Rand_k(\phi_k)
\end{aligned}
\tag{6}
$$

For each line segment I_k, $I_{\min,k}$ is the local minimum of I_k, and $Rand_k(\phi_k)$ is a random variable that represents how much a small part of a signal varies between 0 and ϕ_k. Hence, after applying local normalization $LN(.)$, $I_{\min,k}$ will be significantly reduced and the normalized signal can be expressed as follows:

$$
\begin{aligned}
LN(I(x, y)) &= LN(\{I_k(x, y), \ k = 1, 2, ..., S\}) \\
&= LN(\{Rand_k(\phi_k), \ k = 1, 2, ..., S\})
\end{aligned}
\tag{7}
$$

Therefore, the mean of $LN(I(x, y))$ can be derived by:

$$
\begin{aligned}
&Mean(LN(I(x, y))) \\
&= Sum(LN(\{Rand_k(\phi_k), \ k = 1, 2, ..., S\}))/S,
\end{aligned}
\tag{8}
$$

where $Sum(.)$ represents the summation process. According to the central limit theorem, if S is large, $Sum(LN(\{Rand_k(\phi_k), \ k = 1, 2, ..., S\}))$ will be normally distributed. Therefore, the mean of the normalized signal $LN(I(x, y))$ will be close to the center of a dynamic range. On the other hand, since $L'(x, y)$ can be considered a low-pass filtered version of the normalized signal $LN(I(x, y))$, $L'(x, y)$ will definitely satisfy the constraint set by Equation (3). Note that, although $LN(I(x, y))$ can satisfy the constraints set in Equations (3), (4), and (5), components that have larger gradient values in an image $I(x, y)$, expressed as $L(x, y)$, are removed simultaneously. Since this situation is definitely undesirable, we introduce an additional attenuation ratio T to multiply the lower bound intensity $I_{\min,k}$ in the local normalization process. This ensures that $L(x, y)$ can be

preserved, but it will be compressed to $1-T$. The effect of adding the ratio T is that the value of $Mean(LN(I(x,y)))$ will be shifted slightly away from the center of the dynamic range. However, as the shift will not move $Mean(LN(I(x,y)))$ to either of the extreme values of the dynamic range, the constraint set by Equation (3) still holds.

In order to ensure the image quality, we also introduce an adaptive contrast assessment mechanism to preserve or enhance visual details. This is done by adjusting the original good contrast and the enhanced contrast adaptively. To build the mechanism, we need to compute an exponent factor. We describe how to determine this factor in the next subsection. With the above mentioned mechanism, we can ensure that the contrasts of the processed image are better defined than those of the original image.

2.2. The Proposed Tone Reproduction Scheme

Based on the concepts described in the previous section, we propose the following tone reproduction scheme:

$$I'(x,y) = I(x,y) \times E(x,y)^{C(x,y)},$$ (9)

where $I'(x,y)$ is an enhanced image signal. $I(x,y) \times E(x,y)$ is the locally normalized version of $I(x,y)$; hence $E(x,y)$ is the local normalization ratio kernel. In our design, for an image $I(x,y)$, $E(x,y)$ is derived by the following equation:

$$E(x,y) = \frac{I(x,y) - I_{min} \times T}{I_{max} - I_{min} \times T + \varepsilon} \times \frac{G}{I(x,y)}.$$ (10)

As mentioned earlier, we modify the normalization equation by adding an attenuation ratio T (ranging from of 0 to 1) to our tone reproduction scheme. I_{max} and I_{min} are the respective local maxima and minima of an image signal; G is the full size of the dynamic range; and ε is an offset to avoid the divide-by-zero situation. In our scheme, an exponent factor is added to balance the original good contrast and the contrast enhanced by our

method. By applying the adaptive contrast assessment mechanism introduced in the previous subsection, we have $C(x, y)$, an adaptive contrast assessment factor, which is defined as follows:

$$C(x, y) = Gaussian(\arg\{Lap(I), Lap(I')\}), \tag{11}$$

where $\arg\{a,b\} = 0$ when $a > b$, and $\arg\{a,b\} = 1$ when $a \leq b$; $Lap(.)$ is the Laplacian operator:

$$Lap(I) = \frac{\partial^2 I}{\partial x^2} + \frac{\partial^2 I}{\partial y^2};$$

and $Gaussian(.)$ denotes the Gaussian operator. Let the width of a filter be 1/10 of the longest side of an image and its corresponding standard deviation be 1/5 of the width (which results in a flat Gaussian filter) to ensure that $C(x, y)$ will change smoothly. With $C(x, y)$, our proposed mechanism can enhance the low contrast regions of an image, while preserving the details of high contrast regions. Since the local normalization process normalizes an image toward its local maxima and local minima surfaces, we can think of it as partitioning an image into densely connected piecewise segments, and then normalize those segments. We can expand the expression shown in Equation (6) and express it mathematically as $E(x, y) = \{E_k(x, y), \ k = 1, 2, ..., S\}$. Combining Equations (1) and (10) we have:

$$E_k(x, y) = \left(\frac{G}{G_{L,k}}\right) \times \frac{\left[1 - \frac{I_{min,k} \times T}{I_k(x, y)}\right]}{(1 + \varepsilon / G_{L,k})}, \tag{12}$$

where $G_{L,k} = I_{max,k} - I_{min,k} \times T$. Let $\eta_k(x, y)$ be the intensity difference between $I_k(x, y)$ and $I_{min,k}$; then we have

$$I_k(x, y) = I_{min,k} + \eta_k(x, y), \tag{13}$$

$$I_k'(x, y) = I_k(x, y) \times E_k(x, y)^{C_k(x,y)}$$
$$= I_k(x, y) \times \{\frac{G}{G_{L,k}} \times \frac{1 - T \times \left(1 + \frac{\eta_k(x, y)}{I_{min,k}}\right)^{-1}}{(1 + \frac{\varepsilon}{G_{L,k}})}\}^{C_k(x,y)}. \tag{14}$$

Next, we consider the following three cases of ordinary target regions for enhancement: Case 1: a region with low local contrast and high local luminance; Case 2: a region with low local contrast and medium local luminance; and Case 3: a region with low local contrast and low local luminance. In the first case, the local luminance is high, so $I_{\min,k}$ can be much larger than $\eta_k(x, y)$; therefore,

$$V'_{Case1}(x, y) = \frac{I'_{Case1}(x, y)}{I_{Case1}(x, y)} = \{\frac{G \times (1-T)}{G_{L,k} + \varepsilon}\}^{C_k(x,y)}. \tag{15}$$

In the second case, $I_{\min,k}$ is comparable to $\eta_k(x, y)$; therefore,

$$V'_{Case2}(x, y) = \{\frac{G \times \left(1 - \frac{T}{\left(1 + \eta_k(x, y)/I_{\min,k}\right)}\right)}{G_{L,k} + \varepsilon}\}^{C_k(x,y)}. \tag{16}$$

In the third case, $\eta_k(x, y)$ is more dominant than $I_{\min,k}$; therefore,

$$V'_{Case3}(x, y) = \left[G \times \left(1 - \frac{T \times I_{\min,k}}{\eta_k(x, y)}\right) \middle/ (G_{L,k} + \varepsilon)\right]^{C_k(x,y)}. \tag{17}$$

By carefully selecting T and ε, our proposed algorithm can guarantee that V will be greater than 1 in all cases. In the scheme, ε is a small constant offset to ensure that the divided-by-zero situation will not arise. For example, we set $T = 0.8$ and $\varepsilon = 3$. When $V > 1$, the above three cases can be interpreted as follows. In the first case, since the local luminance is high, $L_1(x,y)$ tends to decrease. However, as $V'_{case1} > 1$, $R_1(x,y)$ tends to be greater than 1. In the second case, the resulting V'_{case2} will be quite large with our settings. Even with a medium local luminance, $V'_{case2}/L_2(x,y) = R_2(x,y)$ would still be much larger than 1. The third case is similar. Since a dominating $\eta_k(x, y)$ would make V'_{case3} a large value compared to 1, it is reasonable that $L_3(x,y)>1$ and $R_3(x,y)>1$ to ensure a large V'_{case3}. To sum up, the proposed image enhancing process clearly satisfies the constraints set in Equations (3), (4), and (5), i.e., it preserves the details and restores the visibility of a processed image. More supporting details and figures are provided in Section 2.4.

2.3 Quality Evaluation

To evaluate the performance of our tone reproduction scheme, we introduce a visual detail assessment mechanism based on the JND profile. In [8], Chou and Li proposed a way to estimate the JND profile of the human visual system. With the JND profile, we can determine the regions in which the image details are visible to a human observer and thereby obtain the percentage of perceptible visual details. Note that in our estimation of the perceptible percentage, we do not consider the effect of spatial masking. Instead, we only consider the relationship between the visibility threshold and the background luminance, which is an underlying technique described in the JND profile. The visibility threshold is expressed in Equation (18), while the curve of the visibility threshold is depicted by the blue curve in Figure 1. We use the Laplacian operator to calculate the contrast value of all the pixels in an image, and then use the curve of the visibility threshold to determine whether they are visible or not. With this JND profile, we can quantitatively compute the proportion of an image that is actually restored. The JND profile we adopted from [8] is expressed as follows:

$$
\begin{aligned}
JND(x, y) &= f\ (bg(x, y)) \\
&= \begin{cases} T_0 \cdot (1 - (bg(x, y)/127)^{1/2})) + 3 & \text{for } bg(x,y) \leq 127 \\ \gamma \cdot (bg(x, y) - 127) + 3 & \text{for } bg(x, y) > 127 \end{cases}
\end{aligned}
\tag{18}
$$

where $bg(x, y)$ is the average background luminance, and T_0 and γ are set at 17 and 1/2, respectively.

To further explain how the parameter set is determined and how the quality of an image is improved after applying our tone reproduction algorithm, we synthesize a test image by combining different image intensities to produce possible contrasts. As shown in Figure 2 (a), the synthesized test image consists of a vertical base gradient with the background luminance ranging from 0 to 255 (top to bottom) and randomly generated details whose intensity ranges from 0 to 255(left to right). The purpose of applying local normalization to this image is to determine if our algorithm can enhance various levels of contrast under different background luminance levels. As Figure 2 (b) demonstrates, the visual clarity is significantly enhanced, and the parts of the smooth gradient are also preserved. In the next section, we apply the quality evaluation scheme on this synthetic image to perform quantitative analysis.
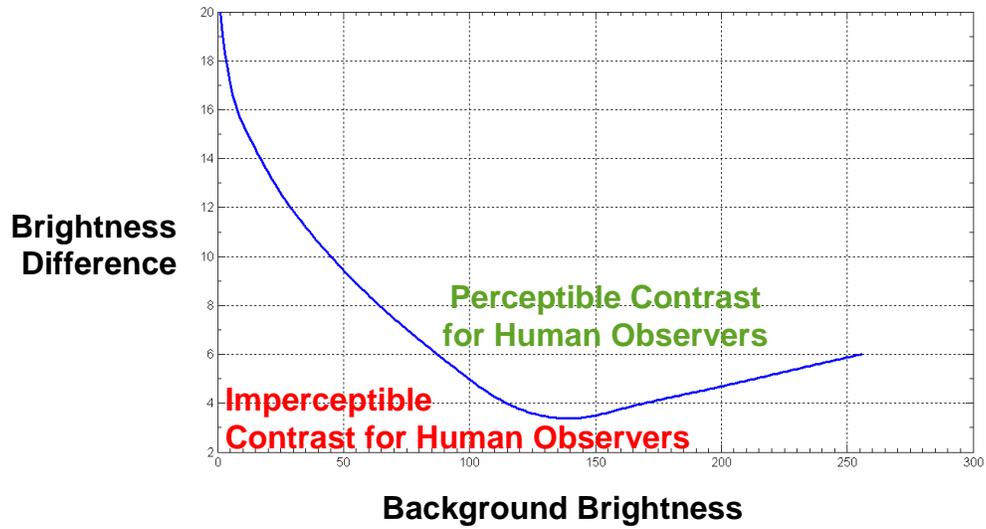
Figure 1. JND profile of the human visual system.

(a) Test image   (b) Resulting image
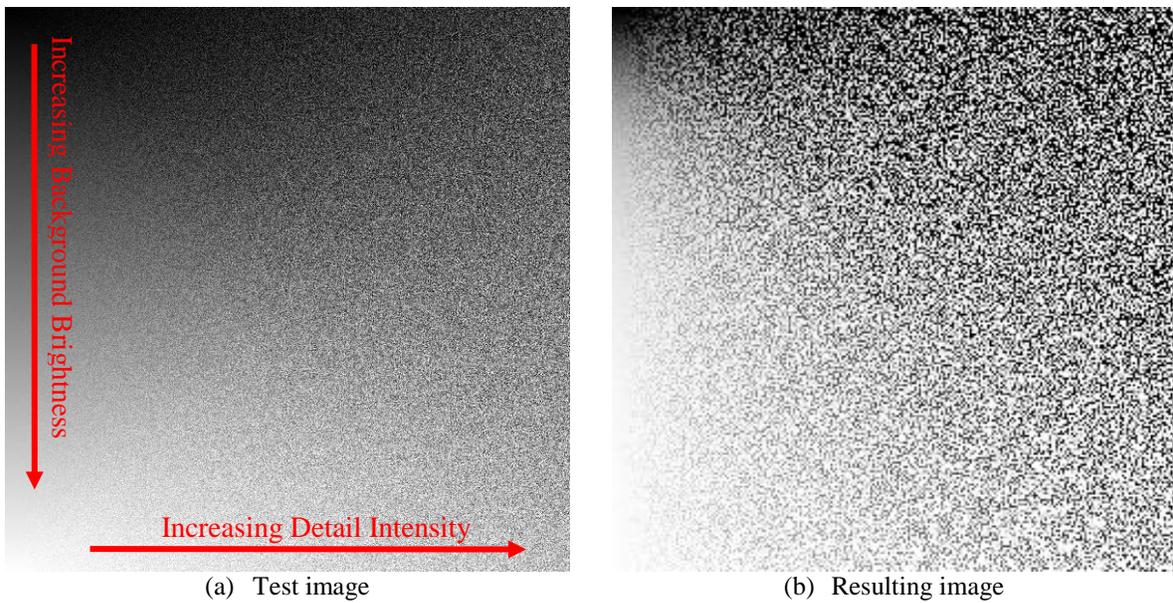
Figure 2. (a) The synthesized test image; and (b) the resulting image after applying local normalization (b).

2.4 Scheme Design Details

In this subsection, we provide further details about how we systematically determine a good parameter set based on two primary guidelines: **increasing the degree of detail visibility** and **reducing the effect of artifacts**, such as the effect of noise, the effect of gradient reversal, and the halo effect.

By Equation (18), we can clearly define an approximate JND profile of the human visual system. Therefore, by varying the two parameters T and ε mentioned in the previous section (Equation (10)), we hope to achieve a high estimated perceptible percentage of an image. On the other hand, to preserve a better visual impression, we want to reduce the amount of perceived noise. Although the noise will inevitably be amplified through our local normalization process, we choose the parameters carefully to ensure the amplified noise will always be below the level in the JND profile. This concept is similar to the idea used in transparent coding.

2.4.1 Noise Reduction

Noise reduction is considered a crucial step in image quality improvement. To achieve it, we first locate the average noise level of various digital camera models (ranging from high-end digital single-lens reflex cameras to popular compact units). Based on the statistics reported in [9], we set the average noise level as 3 for an 8-bit imaging system, and consider an image's visual details that fall below this level as noise. As shown in Figure 3 (a), the vertical line represents this average noise level. Thus, we consider that the region to the right of this boundary contains valuable visual details, while the region to the left contains unwanted noise. Then, we adopted the JND profile to estimate the perceptible percentages of the above two regions (as shown in Figure 3). In this way, we can determine an appropriate set of parameters to maximize the visual details of an image and simultaneously ensure that noise in the image is minimized or imperceptible.

To determine the percentage of the perceptible details of an image, we perform the following experiments. First, we vary T in Equation (10) to observe the change in the percentage of visual detail. As shown in Table 1, when T varies between 0.1 and 0.9, the percentage of visual detail of regions with intensity values higher than the JND profile level increases by about 0.2%. However, for those regions whose intensity values are lower than the

JND profile level, the percentage increases by about 7%. Hence, the amount of undesirable noise increases faster than the amount of restored details when we try to maximize the visual details by varying T between 0.1 and 0.9. As perceptions of visual pleasantness are closely related to the SNR of an image, we would rather make T small so that an image is more visually pleasing. Hence, we set T at 0.1.

Resulting Image	Perceptible Details (estimated by JND profile)

Sampling along original detail level = 3	Sampling along original detail level = 3
(a)	(b)
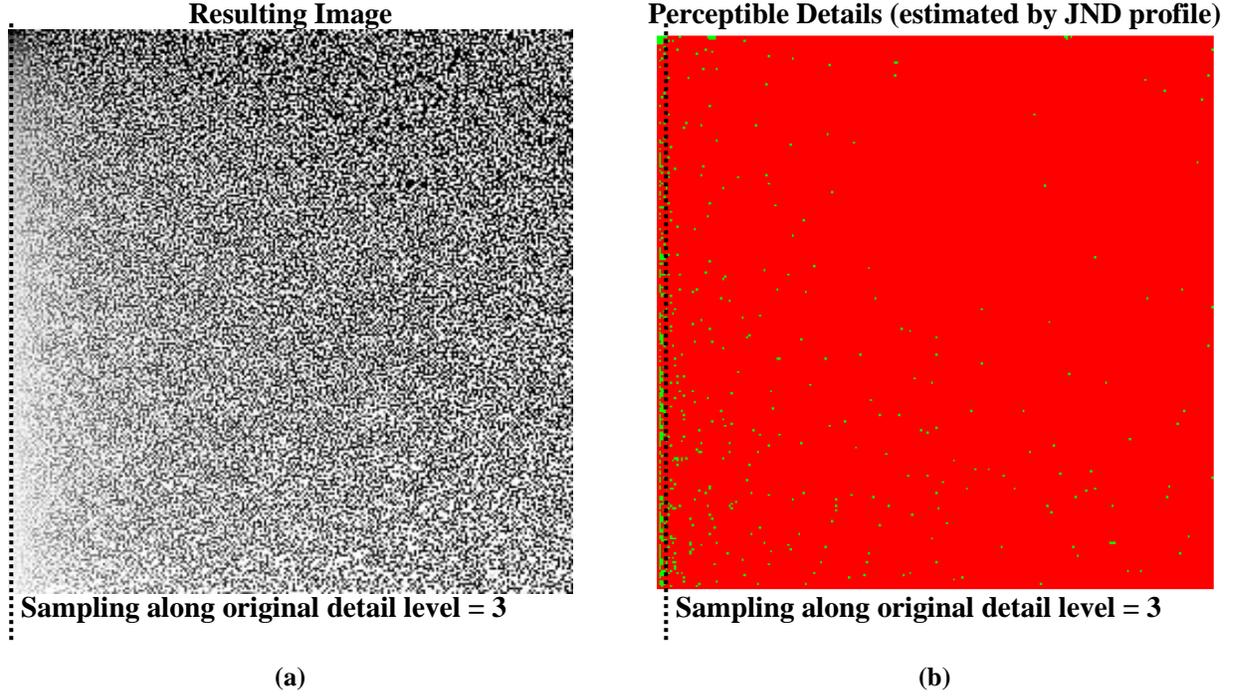
Figure 3. (a) The enhanced result; and (b) the estimation of perceptible details (the green regions indicate imperceptible areas).

Having explained the general principle of how to determine T, we now consider the offset ε. In our scheme, we make ε adaptive:

$$\varepsilon = v \times (s - \min(s)) + 0.1, \quad where \quad s = 1/(I_k(x,y)+1). \tag{19}$$

As a result, ε will be dominant when $I_k(x,y)$ is low. This setting also helps reduce visible noise artifacts. For now, ε becomes a function of v. We illustrate the difference between using constant and adaptive ε in Figure 4. In the figure, the green curves are the gradients of the average luminance using the signals sampled when the intensity level of added detail is equal to 3 (as shown in Figure 3 (a)); the blue curves are the enhanced signals; the brown curves are the average luminance levels of the enhanced signals; and the red curves are the gradients of the average luminance. In Figure 4 (a), as a constant ε is used, the gradients of the average luminance (the red

curve) decrease from the maximum value to smaller values as the average luminance level increases from extremely low to higher levels (along the x axis in Figure 4 (a)). However, in Figure 4 (b), the gradient of the average luminance using adaptive ε can be controlled to generate a totally different curve. That is, the gradient's value starts from zero and rises to a maximum value when the average luminance level is extremely low (red dotted box in Figure 4 (b)). The magnified views of Figures 4 (a) and (b) are shown in (c) and (d) respectively. In other words, using adaptive ε effectively suppresses noise when the average luminance level is very low. In Figures 4 (e) and (f), the blue curve depicts the JND profile curve and the red curve (with magnitude fluctuation) is the absolute magnitude obtained by subtracting the enhanced signal (blue curves in Figures 4 (a) and (b)) from its corresponding average luminance (red curves in Figures 4 (a) and (b)). From the curves enclosed by the red dotted boxes shown in Figures 4 (e) and (f), it is clear that using a constant ε cannot suppress the perceptible noise when the average luminance level is low (Figure 4 (e)). On the other hand, an adaptive ε can effectively reduce such noise in those low average luminance regions (Figure 4 (f)).

Table 1. Perceptible details of different regions by varying the parameter values.

Regions whose intensity is above the JND profile level (the higher, the better)					
Perceptible Details (%)	T=0.1	T=0.3	T=0.5	T=0.7	T=0.9
v=1	99.6629	99.6693	99.7374	99.8006	99.8622
v=10	99.6126	99.6548	99.7423	99.7990	99.8622
v=100	99.6061	99.6888	99.7488	99.7553	99.8703
v=1000	99.5802	99.6483	99.6985	99.7553	99.8104
Regions whose intensity is below the JND profile level (the lower, the better)					
Perceptible Details (%)	T=0.1	T=0.3	T=0.5	T=0.7	T=0.9
v=1	91.0156	92.8906	94.8698	96.2760	98.2552
v=10	90.8854	93.1771	95.1302	97.0313	98.9063
v=100	90.7552	92.2656	94.4531	96.2500	98.2031
v=1000	90.3646	91.6667	93.3854	94.5573	95.9896

As mentioned in Section 2.4, although it is inevitable that noise will be amplified through our local normalization process, if we choose the parameter values carefully the noise will be invisible/imperceptible (by always keeping the amplified noise below the level in the JND profile). Thus, as *T* is already decided, we vary *v* from 1 to 10000 and sample along the vertical line where the added detail intensity level is 3. Then, we calculate the signal fluctuation after the enhancement process is finished.
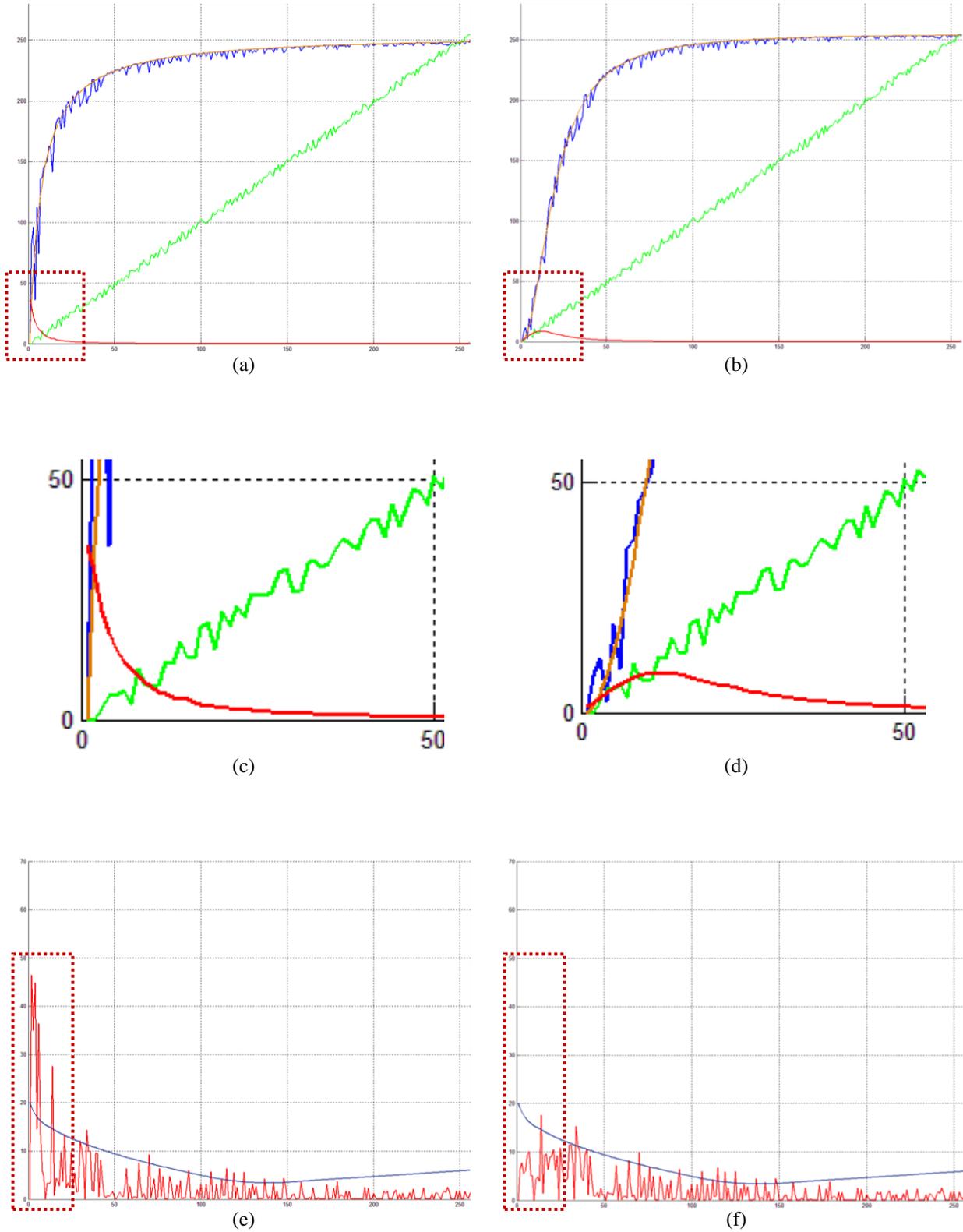
Figure 4. Comparison of the noise suppression effect using a constant ε : (a), (c) and (e), and using an adaptive ε : (b), (d) and (f). (c) and (d) are magnified version of (a) and (b), respectively.

As the allowed fluctuation in amplitude should be confined by the JND profile to ensure that all noise falling below the JND profile remains imperceptible, we find that the threshold for v should be greater than 400, as shown in Figures 5 (a) and (b). Significantly, we also find that the lower the threshold of v, the greater amount of visual details that can be preserved. Thus, setting v as 400 is reasonable because it achieves a balance between detail visibility and noise reduction. Moreover, in Figures 5 (c) and (d), it is clear that the enhanced signal will be perceptible (as the signal fluctuation is higher than the JND profile) when the randomly generated detail level is 8 or higher. However, when dealing with certain kinds of images (such as photographs captured by a phone camera), the noise could still be perceptible in some regions because the noise level is actually higher than our assumed average.

(a) $v =$**10**

(b) $v =$**400**

(c)

(d)
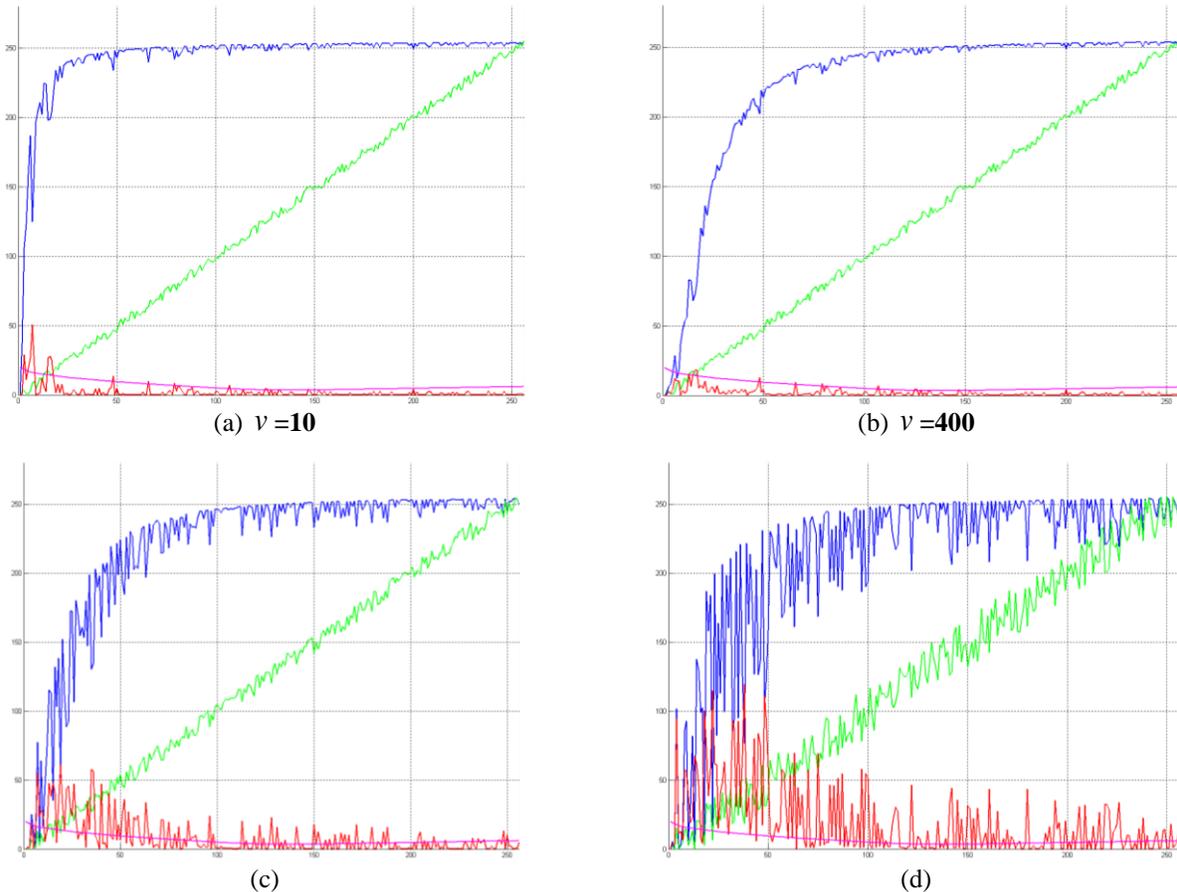
Figure 5. Noise reduction using different v . (a) Perceptible noise occurs in the low brightness region when $v =$10 (added detail intensity=3). (b) Perceptible noise suppressed in the low brightness region when $v =$400 (added detail intensity=3). (c) Details are enhanced and become perceptible when $v =$400 (added detail intensity=8). (d) Details are enhanced and become perceptible when $v =$400 (added detail intensity=20).

Figures 6 and 7 demonstrate the effect of noise reduction. In our test image set of more than 250 images, using the above two pre-determined parameters (T and v), our tone reproduction algorithm recovered more than 84% of the visual details of an image on average.

2.4.2 Non-Gradient Reversal and Human Visual System Similarities

From Figure 5, it is clear that the processed signal exhibits gamma function-like responses. Since the perceptual response of the human visual system is also a gamma function-like, such a characteristic demonstrates that our proposed tone reproduction scheme can produce enhanced images close to how humans actually perceive images. Moreover, in our experience, it is very common for people to feel intuitively that information is hidden in the dark regions, rather than the bright regions of an image. People are more interested in exploring the visual details in low brightness regions, because it is natural to think that such regions are imperceptible. As the gamma function increases monotonically, the gradient of the processed signal will follow that of the original signal and the effect of gradient reversal will not be evident in our scheme.

2.4.3 Reducing the Halo Effect

In addition to the above artifacts, we also consider the halo effect, which often occurs in existing tone mapping/reproduction algorithms and degrades the quality of an image. Although there is still no firm conclusion about how the halo effect occurs, we found that it usually occurs when the image enhancement process involves low-pass filtering. A low-pass filter is usually introduced to either "smooth" the region boundaries or perform a process locally. This explains why the halo effect occurs along the boundaries between a processed region and a non-processed region. However, the halo effect is minimized in our results because our local normalization scheme does not employ low-pass filtering. Furthermore, to suppress possible causes of the halo effect, we also consider non-linear image processing techniques [10, 11] to implement the smoothing process in order to reduce noise.

Figure 6. Noise reduction using different v. (a) Perceptible noise occurs in the low brightness region when v =10. (b) Perceptible noise is significantly suppressed in the low brightness region when v =400.
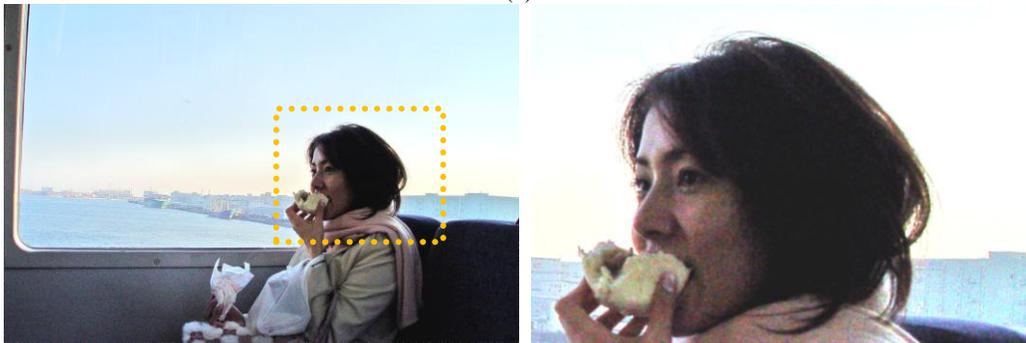
Figure 7. Noise reduction using different v. (a) Perceptible noise occurs in the low brightness region when v =10. (b) Perceptible noise is significantly suppressed in the low brightness region when v =400.

3. EXPERIMENT RESULTS

To test the effectiveness of our method, we conducted experiments on a set of images acquired under various shading/lighting conditions. All the image results demonstrated in this paper were processed with two default parameters (T=0.1 and v=400). Figures 8 (a), (b), (c), and (d) show four test images in which the lighting conditions range from simple to complex; and Figures 8 (e), (f), (g), and (h) show the respective tone reproduced results. Clearly, the details of the tone reproduced images in Figures 8 (f) and (g) are greatly enhanced. Figures 8 (e) and (h) show that it is possible to recover the visual details of the heavily shaded areas in the tone reproduced images. Note that the halo effect was substantially reduced because we did not use a low-pass filter in the local normalization process.

(a)	(b)	(c)	(d)
(e)	(f)	(g)	(h)
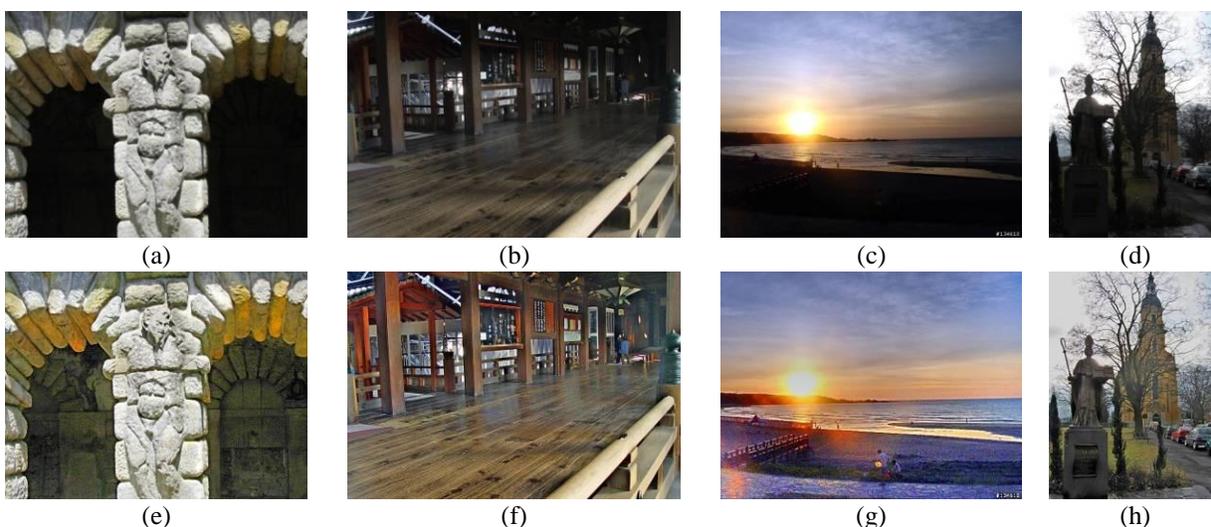
Figure 8. Test images and results with lighting/shading conditions ranging from simple (left) to complex (right). (a)-(d), original images; (e)-(h), enhanced images.

Figures 9 (c)-(f) show some tone reproduced results after applying a variety of existing algorithms to the original image in Figure 9 (a). Figure 9 (b) shows the result obtained after applying our algorithm, while Figures 9 (c), (d), (e), and (f) are the results obtained by applying the tone reproduction algorithms proposed by Reinhard (2004), Fattal (2002), Pattanaik (2000), and Drago (2003), respectively. Since the compared algorithms require the selection of a good parameter set to obtain visually pleasing results, we fine tuned each algorithm's parameters

to obtain a near optimal set of results in the experiment. In contrast, our method does not require manual parameter selection.

The results obtained after applying a perceptibility test to various contrast reduced images are shown by the images with blue labels in Figure 9. The higher percentage means that greater amounts of an image's details are perceptible. For example, in this set of experiments, our method restores the details in the image such that 90.58% of the image is visible to human eye. This result yields the highest number of image detail regions, and the highest percentage among the compared methods.
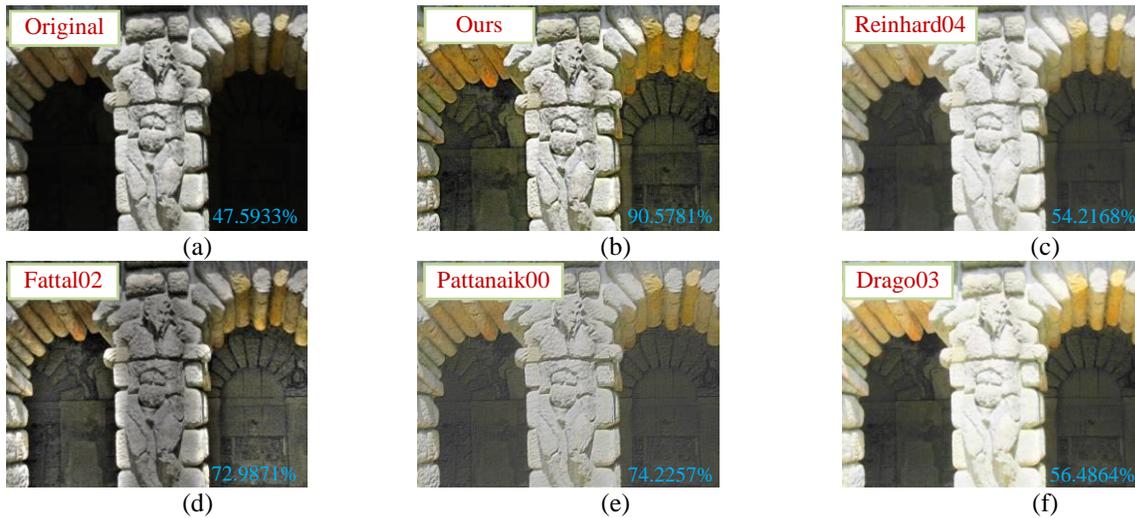
Figure 9. Comparison of various tone reproduction algorithms. (a) Original, (b) our method, (c) Reinhard (04), (d) Fattal (02), (e) Pattanaik (00), and (f) Drago (03).

In terms of perceptibility, among the above evaluation metrics, Fattal *et al*.'s method generally yielded the second best results on all our test sequences, which contained more than 250 images. Figure 10 provides a more detailed comparison of our results and those of Fattal et al.'s method. From the perceptible details, the contrast distributions, and the difference in contrast distribution shown in the figure, it is clear that our algorithm can restore a much larger percentage of an image's details.

The images in Figure 11 demonstrate the efficacy of our smart tone reproduction scheme. In many of the enhanced images of the test image set, the percentage of perceptible detail of the restored regions is as high as 93% using the default parameter set described earlier. The results show that our tone reproduction scheme is robust and accurate.

It should be noted that no single tone reproduction algorithm can be applied to all images. The proposed scheme simply emphasizes the effectiveness of preserving the visual information of an arbitrary image. Even so, the experiment results show that, overall, the performance of our algorithm is superior to that of existing approaches.

Resulting Image	Perceptible Detail (Green: pixel-wise contrasts that fall below the JND profile)	Contrast Distribution (The red curve is the JND profile)	Contrast Distribution Difference (Our method and Fattal's method)	Perceptible Detail %
Fattal02				72.9871%
Ours				**90.5781%**
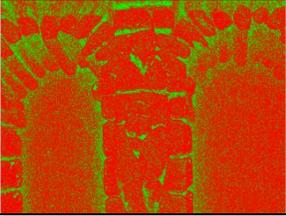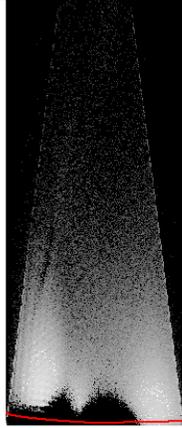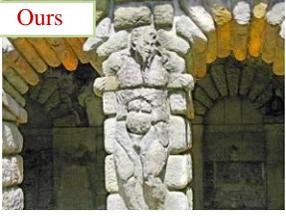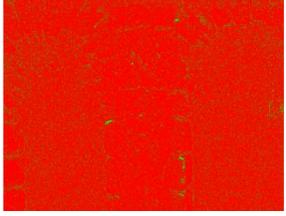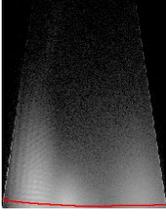
Figure 10. Comparison of the percentage of perceptible details processed by the proposed tone reproduction algorithm and Fattal's algorithm. Note that the contrast distribution of our method spreads significantly wider than that of Fattal's method.

4. CONCLUSION

We have proposed a robust tone reproduction scheme based on image model and image enhancement concepts to obtain a more balanced visual representation. When applied to our test data, which includes a range of lighting conditions and shading effects, our tone reproduction algorithm achieves excellent detailed reproductions without the need for further user parameter adjustments (if the default settings are used). For most images, the proposed tone reproduction scheme is precise and robust, and the parameters used in our algorithm do not have to be adjusted. Moreover, the enhanced images processed by our intuitive scheme are close to the quality that most people expect in a natural photograph. (Please see Fig. 11.)

Original Image and Perceptible Details (red regions)	Result Image and Perceptible Details (red regions)
Perceptible Detail: 64.3343%	Perceptible Detail: 90.4098%
Perceptible Detail: 55.3543%	Perceptible Detail: 92.1788%
Perceptible Detail: 36.7549%	Perceptible Detail: 94.6199%
Perceptible Detail: 53.0243%	Perceptible Detail: 94.6000%
Perceptible Detail: 28.6945%	Perceptible Detail: 93.0743%
Perceptible Detail: 33.1167%	Perceptible Detail: 82.7706%
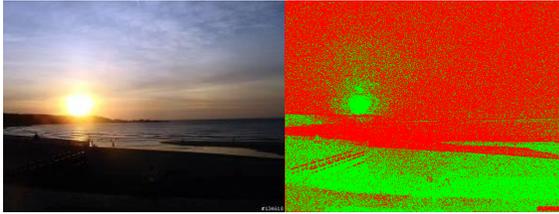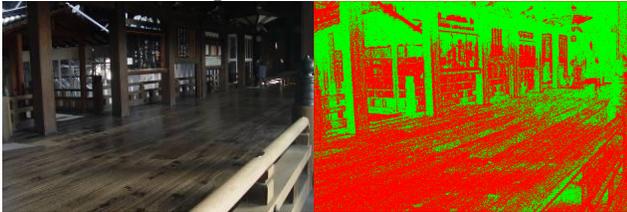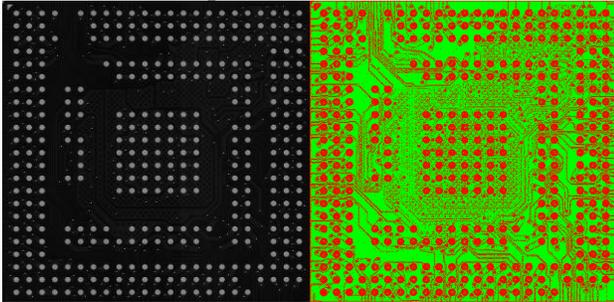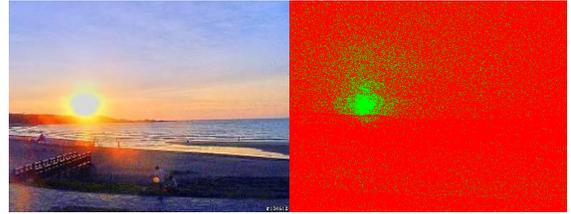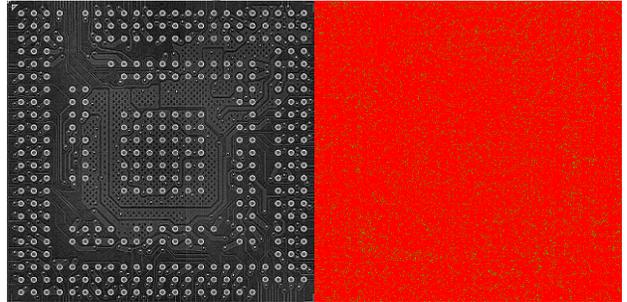
Figure 11. Comparison of the original images and the enhanced images.

5. ACKNOWLEDGEMENT

6. REFERENCES

[1] S. Pattanaik, and H. Yee, "Adaptive gain control for high dynamic range image display," *Proc. Spring Conf. Computer Graphics*, pp. 83-87, 2002,.

[2] F. Durand, and J. Dorsey, "Fast bilateral filtering for the display of high-dynamic-range images," *Proc. SIGGRAPH 2002*, pp. 257–266, 2002.

[3] R. Fattal, D. Lischinski, M. Werman, "Gradient domain high dynamic range compression," *Proc. SIGGRAPH 2002*, pp. 249-256, 2002.

[4] F. Drago, K. Myszkowski, T. Annen, and N. Chiba, "Adaptive logarithmic mapping for displaying high contrast scenes," *Proc. of EUROGRAPHICS 2003*, pp. 419-426, 2003.

[5] E. Reinhard, and K. Devlin, "Dynamic range reduction inspired by photoreceptor physiology," *IEEE Trans. Vis. Comput. Graph.,* vol. 11, pp. 13-24, 2005.

[6] G. Krawczyk, K. Myszkowski, and H.-P. Seidel, "Lightness perception in tone reproduction for high dynamic range images," *Proc. of EUROGRAPHICS 2005,* vol. 24, pp. 635-645, 2005.

[7] H.T. Chen, T.L. Liu, and C.S. Fuh, "Tone reproduction: a perspective from luminance-driven perceptual grouping," *Int. J. Comput Vision.,* vol. 65, pp. 73-96, 2005.

[8] C. H. Chou, and Y. C. Li, "A perceptually tuned subband image coder based on the measure of just-noticeable-distortion profile," *IEEE Trans.on Circuits Syst. Video Technol.,* vol. 5, pp. 467-476, 1995.

[9] Dpreview Website: http://www.dpreview.com

[10] C.-J. Sze, H.-Y. Mark Liao, and K.-C. Fan, "A new image flux conduction method and its application to selective image smoothing," *IEEE Trans. on Image Processing*, vol. 10, no. 2, pp. 296-306, 2001.

[11] C. -C Shih, H.-Y. Mark Liao, and C.-S Lu, "A New Iterated Two-band Diffusion Equation :Theory and Its Application," *IEEE Trans. on Image Processing*, vol. 12, no. 4, pp. 466-476, 2003.